Spin-Orbit-Coupled Correlated Metal Phase in Kondo Lattices: An Implementation with Alkaline-Earth Atoms

L. Isaev, J. Schachenmayer, and A. M. Rey

Phys. Rev. Lett. **117**, 135302 — Published 20 September 2016

DOI: 10.1103/PhysRevLett.117.135302

Spin-orbit coupled correlated metal phase in Kondo lattices: an implementation with alkaline-earth atoms

L. Isaev, J. Schachenmayer, and A. M. Rey
JILA, NIST, Department of Physics & Center for Theory of Quantum Matter, University of Colorado, 440 UCB, Boulder, CO 80309, USA

We show that an interplay between quantum effects, strong on-site ferromagnetic exchange interaction and antiferromagnetic correlations in Kondo lattices can give rise to an exotic spin-orbit coupled metallic state in regimes where classical treatments predict a trivial insulating behavior. This phenomenon can be simulated with ultracold alkaline-earth fermionic atoms subject to a laser-induced magnetic field by observing dynamics of spin-charge excitations in quench experiments.

PACS numbers: 72.15.-v, 75.20.Hr, 67.85.-d, 37.10.Jk

Introduction.– The behavior of correlated quantum systems can rarely be understood in terms of individual atoms or electrons, and instead is determined by a competition between their strong interactions and kinetic energy [1]. This interplay often places states with fundamentally different properties energetically close to each other, and hence makes the system highly sensitive to external controls such as pressure, or magnetic field [2].

A paramount example of correlation-driven tunable phenomena is the colossal magneto-resistance in transition-metal oxides, e.g. manganites [3, 4]. Properties of these materials are governed by the ferromagnetic Kondo lattice model (FKLM) which includes competition between kinetic energy of itinerant electrons and their Hund exchange coupling with localized spins [5, 6]. This interaction often exceeds the conduction bandwidth and ensures that only on-site triplets, i.e. electrons whose spins are aligned with local magnetic moments, can exist at low energy. For classical core spins ($S \gg 1$), an effective electron hopping amplitude between two lattice sites strongly depends on the magnetic background: it is largest when local spins on the two sites are parallel, and vanishes for anti-parallel [antiferromagnetically (AF) ordered] local moments [7, 8]. As a result, the conductivity of a system becomes highly sensitive to small variations in the magnetic texture, e.g. caused by an external magnetic field. This so-called double-exchange (DE) physical picture remains qualitatively valid when quantum fluctuations of the local magnetism are taken into account [9–13] and in the extreme quantum case $S = \frac{1}{2}$ [14].

Nevertheless, even early works [8] hinted at a breakdown of the DE semiclassical description in the presence of strong AF correlations between local spins when they form at least short-range Néel order. While in an ideal antiferromagnet an electron can not move, it still gains energy via smooth deformations of the Néel background. Quantum fluctuations allow local spins to form singlets with mobile fermions and further distort the AF texture.

In the present Letter we demonstrate that quantum nature of the local magnetism *dramatically affects* physics of a FM Kondo lattice with AF correlations between core spins [Fig. 1(a)]. We focus on a $S = \frac{1}{2}$ FKLM in the strong-coupling regime, when Hund and AF interactions exceed the electron bandwidth, and show that the AF environment of each core moment frustrates the on-site Hund exchange V [Fig. 1(b)]. Properties of the model are controlled by a competition between V and an energy scale Ω of the antiferromagnetism. When these energies are significantly different, the system is an insulator with localized band electrons. However, near the resonance $V \approx \Omega$, the AF and Hund interactions effectively cancel each other allowing quantum effects to stabilize a new *correlated metal* phase whose quasiparticles admix singlet and triplets states of bare electrons and local spins. These excitations distort the AF order and give rise to a *transverse* (to the Néel vector) magnetization. This resonant behavior is absent in a semiclassical DE theory which predicts an insulating state for any Hund coupling.

The correlated metal phase can be observed in fermionic alkaline-earth atoms (AEAs) [15], such as ^{87}Sr [16] or ^{173}Yb [17–22], in a two-band optical lattice where atoms in the lowest (localized) and higher (itinerant) bands correspond to core spins and mobile fermions, respectively [Fig. 1(c)]. We propose to simulate the AF background with an artificial, laser-induced magnetic field [23–25], which in AEAs can be implemented either using Raman transitions between nuclear spin levels [26] or Rabi coupling of $^1S_0$ and $^3P_0$ electronic clock states [27]. The laser phase can be controlled to vary from one lattice site to the next in a *staggered* fashion, while the Rabi or Raman coupling of relevant atomic states provides a handle of the above singlet-triplet (s-t) resonance.

Correlated metal in a strongly-coupled FKLM.– Let us consider a generic FM Kondo lattice with AF superexchange interactions between core moments:

$$H = -J_0 \sum\nolimits_{\langle ij \rangle} (c^\dagger_{in} c_{jn} + \text{h.c.}) + I_H \sum\nolimits_{\langle ij \rangle} S^z_i S^z_j - \\ - V \sum\nolimits_i \left[\boldsymbol{S}^\perp_i \cdot \boldsymbol{s}^\perp_{ci} + \eta S^z_i s^z_{ci} \right] + R \sum\nolimits_{\langle ij \rangle} n^c_i n^c_j, \quad (1)$$

defined on a bipartite (e.g. square) lattice of Fig. 1(b). Here $c^\dagger_{in}$ creates an electron with spin $n = \uparrow, \downarrow$ (we assume summation over repeated indices) at site $i =$

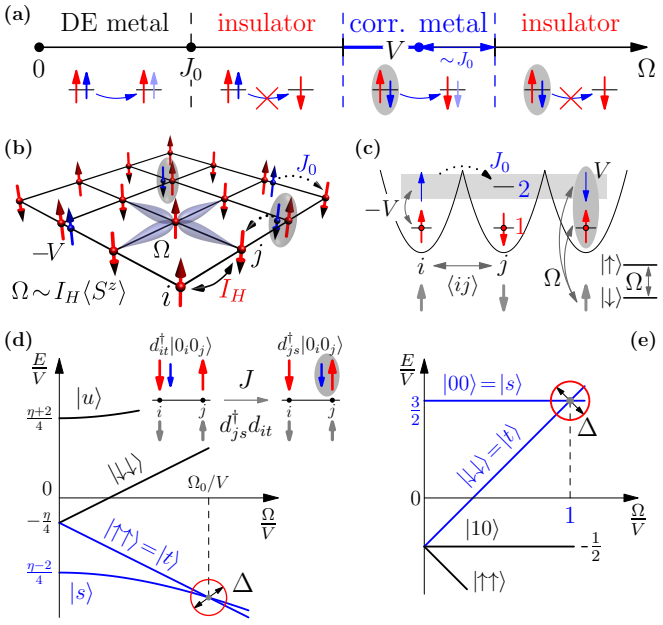

FIG. 1. **(a)** Schematic phase diagram of Eq. (1) with $V \gg J_0$ (Ω is the AF interaction strength), featuring the correlated metal state for strong coupling $\Omega \sim V$. The conventional ferromagnetic (DE) metal occurs at $\Omega \lesssim J_0$. Bottom row: allowed and forbidden (indicated by red crosses) hopping processes. Blue (red) color marks mobile (local) fermions. Light blue spins show final states of itinerant fermions. Gray ellipses denote local entangled singlet-triplet (s-t) states [$|s\rangle$ in (d)]. **(b)** The electronic model of Eq. (1). Color notations are as in (a). Local spins feel a staggered mean-field $\Omega \sim I_H\langle S^z\rangle$ due to the AF background. **(c)** Optical lattice of the AEA setup Eq. (5). Band 1 (2) is localized (itinerant). Gray arrows indicate the laser-induced staggered Zeeman field Ω that splits pseudo-spin $|\uparrow,\downarrow\rangle$ states. Gray ellipse is a spin-singlet state. Other notations are as in (b). **(d)** Energies on an isolated site with one fermion. Blue lines [red circle] indicate the s-t subspace [resonance]. Inset: Hopping of s-t excitations $d_{i\alpha}$ (3). Other notations are as in (a). **(e)** Same as in (d), but for the AEA model (5). The s-t subspace is an excited manifold.

$1 \dots N$. The first line contains nearest-neighbor (NN) hopping J_0 on a link $\langle ij\rangle$, and the AF exchange $I_H > 0$ between local moments $\boldsymbol{S}_i$. The latter are coupled to mobile spins $\boldsymbol{s}_{ci} = \frac{1}{2}c^\dagger_{in}\boldsymbol{\sigma}_{nm}c_{im}$ ($\boldsymbol{\sigma}$ are Pauli matrices) via a FM Hund exchange V with an XXZ anisotropy ($\perp$ denotes xy vector components) $\eta \in [0,1]$ arising from atomic spin-orbit coupling and crystal-field effects. Due to same reasons, the AF interaction is also anisotropic: we consider the simplest Ising limit, but our results are applicable to a general XXZ case. The last term (with $n^c_i = c^\dagger_{in}c_{in}$) is a NN Coulomb repulsion (see below).

We focus on the strong-coupling limit $J_0 \ll I_H$, V and assume that core moments are AF-ordered, $\langle S^z_j\rangle = \langle S^z\rangle e^{i\boldsymbol{Q}\cdot\boldsymbol{x}_j}$ [$\boldsymbol{x}_j \equiv j$, $\boldsymbol{Q} = \pi$ for a one- (1D), (π,π) for a two-dimensional (2D) lattice, etc]. Mobile electrons will form entangled states with local spins, and above certain density $n^c > n^c_{cr}$, destroy the Néel order even for $J_0 \equiv 0$. Hence, the above assumption is valid only in the low-density regime $n^c \ll 1$ when electrons rarely occupy NN sites. This regime is enforced by the repulsion R in Eq. (1). The AF background can be taken into account by performing a staggered transformation:

$$c_{in} = a_{in} \ \ (i \text{ even}); \quad c_{in} = a_{i,-n} \ \ (i \text{ odd});$$
$$\boldsymbol{S}_i = \left(T^x_i, (-1)^i T^y_i, (-1)^i T^z_i\right), \tag{2}$$

where a_{in} and $\boldsymbol{T}_i$ are new mobile fermions and local spins. As a result, the first line in Eq. (1) becomes $-\sum_{\langle ij\rangle}\left[J_0\sigma^x_{nm}(a^\dagger_{in}a_{jm}+\text{h.c.})+I_H T^z_i T^z_j\right]$; other terms remain unchanged with $c_{in} \to a_{in}$ ($\boldsymbol{s}_{ci} \to \boldsymbol{s}_{ai}$) and $\boldsymbol{S}_i \to \boldsymbol{T}_i$.

In this staggered frame, the mean-field Hamiltonian of an isolated site is $H_i = -V\left[\boldsymbol{T}^\perp_i \cdot \boldsymbol{s}^\perp_{ai} + \eta T^z_i s^z_{ai}\right] - zI_H\langle T^z_j\rangle T^z_i$. Here the last term is a molecular field acting on a core spin in the AF environment and z is the lattice coordination number. We assume that $\langle T^z_j\rangle = \langle T^z\rangle > 0$ is j-independent and denote $\Omega = zI_H\langle T^z\rangle$. In a low-density regime, we can focus only on the $n^a_i = 1$ subspace [see Fig. 1(d)]. There are two states with total spin projection $T^z_t = \pm 1$: $|t\rangle_i = a^\dagger_{i\uparrow}|\uparrow\rangle_i$ and $|\downarrow\downarrow\rangle_i = a^\dagger_{i\downarrow}|\downarrow\rangle_i$ and energies $E_{1,2} = -\frac{\eta}{4}V \mp \frac{1}{2}\Omega$; and two $T^z_t = 0$ states: $|u,s\rangle_i = r_\pm a^\dagger_{i\uparrow}|\downarrow\rangle_i \mp r_\mp a^\dagger_{i\downarrow}|\uparrow\rangle_i$ with energies $E_{u,s} = \frac{\eta}{4}V \pm \frac{1}{2}\sqrt{V^2+\Omega^2}$, where $|n\rangle$ is a core-spin state, $r_\pm = \frac{1}{\sqrt{2}}(\cos\vartheta \pm \sin\vartheta)$, $\text{tg}\,2\vartheta = \Omega/V$ (here $|\sigma\rangle_i$ is a shorthand notation for $|\sigma\rangle_i \otimes |0\rangle$, $|0\rangle$ is the a-fermion vacuum). When $\Omega = \Omega_0 = (1-\eta^2)V/2\eta$, $|s\rangle_i$ and $|t\rangle_i$ become degenerate, and at strong-coupling define the local s-t subspace. For $\Omega \sim \Omega_0$ other states, separated by a large gap $\sim \Omega_0$, can be ignored. We represent this Hilbert space with *constrained (no double occupancy) fermions* [28]

$$d^\dagger_{is}|\text{vac}\rangle \leftrightarrow |s\rangle_i, \ \ d^\dagger_{it}|\text{vac}\rangle \leftrightarrow |t\rangle_i. \tag{3}$$

Here $|\text{vac}\rangle = \prod_i |\uparrow\rangle_i$ is a vacuum state with $n^a_i = 0$.

Near the resonance $\Omega = \Omega_0$, the system is described by an effective Dirac-like Hamiltonian

$$H_d = -J\sum_{\langle ij\rangle}[\sigma^x_{\alpha\beta}d^\dagger_{i\alpha}d_{j\beta}+\text{h.c.}] + \Delta\sum_i(n^d_{is} - n^d_{it}), \tag{4}$$

obtained by projecting the Hamiltonian (1) onto s-t subspace (3), i.e. by computing matrix elements of Eq. (1) between states $d^\dagger_{i\alpha}|\text{vac}\rangle$ [29]. In Eq. (4), $J = J_0 r_+$, $\alpha,\beta = s$ or t, and $n^d_{i\alpha} = d^\dagger_{i\alpha}d_{i\alpha}$ (with $n^d_i = n^d_{is} + n^d_{it}$). The first term contains hopping processes [see inset in Fig. 1(d)] that mix local entangled $|s\rangle$ and classical $|t\rangle$ states (3) [because of $\sigma^x_{\alpha\beta}$]. This emergent spin-orbit coupling is rooted in an interplay between strong exchange interactions and quantum fluctuations, and manifests in a *transverse* [orthogonal to Néel vector $\langle S^z_i\rangle$] spin polarization of d-particles: $\boldsymbol{T}^\perp_i = \frac{r_+}{r_-}\boldsymbol{s}^\perp_{ai} = \frac{1}{2}r_+\boldsymbol{\sigma}^\perp_{\alpha\beta}d^\dagger_{i\alpha}d_{i\beta}$. The second term contains an effective detuning $\Delta = \Omega - \Omega_0$ from the s-t resonance and describes a competition between

Hund interaction and AF correlations, both favoring an insulator (at large $|\Delta| \gg J$) with localized fermions. Remarkably, for $|\Delta| \sim J$ the state of the system is driven by a subdominant kinetic-energy scale J, which stabilizes a *correlated metallic phase* with transverse spin excitations. Since the sign of Δ is irrelevant in (4), we will fix $\Delta \geqslant 0$.

The s-t resonance occurs because $\eta < 1$. In the isotropic ($\eta = 1$) strong-coupling case Eq. (1) describes an insulator with localized triplets (similar to a DE model [7]). However, this state is unstable for $\eta < 1$ and $I_H \sim V$. The existence of a s-t resonance does not contradict the "poor man" scaling [30, 31] where the XY exchange V flows to zero at low energies. Indeed, the latter is applicable only at weak coupling $V \ll J_0$, while our theory operates in the opposite, *strong coupling regime* $V \gg J_0$.

Singlet-triplet resonance with AEAs.– We propose to realize the correlated metal phase using AEAs in an optical lattice of Fig. 1(c). The spin-$\frac{1}{2}$ degrees of freedom can be implemented with (i) nuclear spins of atoms in the g electronic state, or (ii) e and g states of nuclear-spin polarized atoms. The Hamiltonian of the system is:

$$H = -J_0 \sum_{\langle ij \rangle} (c^\dagger_{i2n} c_{j2n} + \text{h.c.}) - \sum_i \big[V c^\dagger_{i1n} c_{i1m} c^\dagger_{i2m} c_{i2n} + \\ + \Omega (-1)^i (c^\dagger_{ia\uparrow} c_{ia\uparrow} - c^\dagger_{ia\downarrow} c_{ia\downarrow}) \big] + U \sum_i n^c_{i2\uparrow} n^c_{i2\downarrow}, \qquad (5)$$

where $c^\dagger_{ian}$ creates a fermion at site i in Bloch band $a = 1, 2$ with spin n. Band 1 is localized and contains one atom per site, while the itinerant band 2 has an arbitrary filling and a NN hopping J_0 [32]. The second term in Eq. (5) is an interband exchange interaction. It is FM ($V > 0$) because atoms can experience s-wave collisions only in a spin-singlet state. The third term contains the *staggered* [indicated by $(-1)^i = e^{i\boldsymbol{Q}\cdot\boldsymbol{x}_i}$] Zeeman-like Raman [in case (i)] or direct Rabi [for case (ii)] coupling, with $\Omega > 0$ which simulates the AF environment in Fig. 1(b) [33]. Finally, there is a local repulsion U due to intraband s-wave collisions ($n^c_{ian} = c^\dagger_{ian} c_{ian}$).

Since atoms in band 1 are localized they only contribute spin degrees of freedom, $\boldsymbol{S}_i = \frac{1}{2} \boldsymbol{\sigma}_{nm} c^\dagger_{i1n} c_{i1m}$. Up to a density-density interaction, magnetic terms in Eq. (5) can be rewritten as $-2 \sum_i \big[V \boldsymbol{S}_i \cdot \boldsymbol{s}_{ci} + \Omega (-1)^i (S^z_i + s^z_{ci}) \big]$, where we omitted the band index, $c_{in} \equiv c_{i2n}$. Applying the transformation (2) to Eq. (5), we get rid of $(-1)^i$, and replace $c_{in} \to a_{in}$ ($\boldsymbol{s}_{ci} \to \boldsymbol{s}_{ai}$) and $\boldsymbol{S}_i \to \boldsymbol{T}_i$.

On an isolated site i there are 8 eigenvalues $E_{n^a}(T_t, T^z_t)$ labeled by the total spin T_t, its projection T^z_t and fermion number n^a: $E_0\big(\frac{1}{2}, \pm\frac{1}{2}\big) = E_2\big(\frac{1}{2}, \pm\frac{1}{2}\big) - U = \mp\Omega$, $E_1(0,0) = -3E_1(1,0) = \frac{3}{2}V$ and $E_1(1, \pm 1) = -\frac{V}{2} \mp 2\Omega$. Energy levels with $n^a = 1$ are shown in Fig. 1(e). For small J_0 a mobile atom can propagate only when two or more states are at resonance, i.e. for $\Omega = 0$ or V. The first case is a usual FKLM [5] without AF correlations.

We will concentrate on the second resonance at $\Omega = V$, reached in an *excited* s-t manifold spanned by the local singlet $|s\rangle_i = \frac{1}{\sqrt{2}} [a^\dagger_{i\uparrow} |\downarrow\rangle_i - a^\dagger_{i\downarrow} |\uparrow\rangle_i]$ and triplet $|t\rangle_i = a^\dagger_{i\downarrow} |\downarrow\rangle_i$ [red circle in Fig. 1(e)], and identify these states with the corresponding states (3): now $d^\dagger_{is}$ creates a pure spin-singlet, while $d^\dagger_{it}$ creates a triplet. In an excited manifold, the vacuum state $|\text{vac}\rangle = \prod_i |\downarrow\rangle_i$ has local spins *antiparallel* to Ω. Near the s-t resonance, other singly-occupied states are separated by a gap $\sim V$ and can be ignored, together with the doubly-occupied manifold. The system is described by the effective model (4) with $J = \frac{1}{\sqrt{2}} J_0$, $\Delta = V - \Omega$ [34]. Thus, in a strong-coupling regime $J_0 \ll \Omega$, V and for $\Omega \sim V$, the AEA setup (5) can be used to simulate the s-t resonance dynamics of Eq. (1). For example, the transverse magnetization of a d-particle is now $\boldsymbol{T}^\perp_i = -\boldsymbol{s}^\perp_{ai} = -\boldsymbol{\sigma}^\perp_{\alpha\beta} d^\dagger_{i\alpha} d_{i\beta} / \sqrt{8}$. We focus on the excited s-t manifold because a cold-atom system is usually well-isolated from its environment and can not escape the s-t subspace due to decoherence.

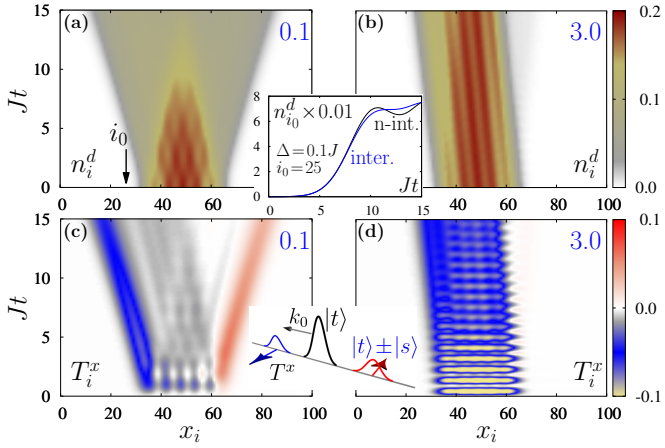

FIG. 2. Propagation of wavepackets with 5 particles. **(a)** and **(b)** show total density $\langle n^d_i(t) \rangle$; **(c)** and **(d)** contain the transverse local-spin polarization $\langle T^x_i \rangle$. Blue numbers in top right corners indicate the detuning Δ/J. Inset: comparison between density evolution at a fixed $x_i = i_0$ [black arrow in panel (a)] in the full model (4) (blue line) and in the case of non-interacting (n-int) d-fermions (black line). The parameters are $N = 101$, $A = 10^{-3} J$, and $k_0 = -20\pi/N$.

Wavepacket dynamics in 1D.– The spin-motion coupling and transverse spin of d-fermions can be probed via propagation of many-body wavepackets. We focus on a 1D case and study dynamics of the model (4) within a time-dependent density matrix renormalization group (t-DMRG) method [35–38]. The initial wavefunction is assumed to contain only triplets and is a ground state (GS) of the Hamiltonian $H_{1D}(t < 0) = -J \sum_i \big[d^\dagger_{it} d_{i+1,t} + \text{h.c.} \big] + A \sum_i \big[x_i - \frac{N}{2} \big]^2 n^d_{it}$ that describes fermions d_{it} in a harmonic trap with $A > 0$. At $t = 0$, the trap is removed, so $H_{1D}(t \geqslant 0) = H_d$, and the packet is accelerated to a momentum k_0 by applying an operator $e^{ik_0 \sum_i x_i n^d_{it}}$.

Fig. 2 shows evolution of five-fermion wavepackets for

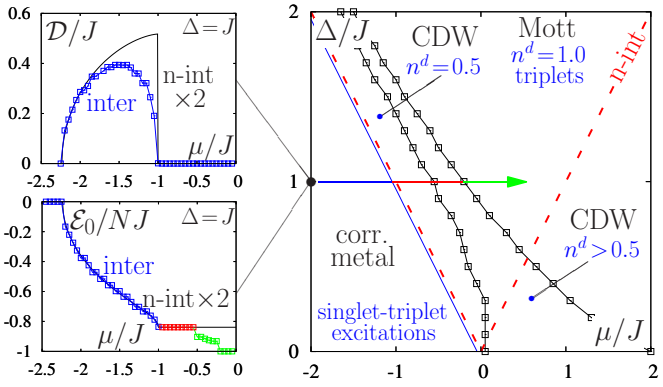

FIG. 3. Phase diagram of the model (4) on a $N = 40$ site chain with periodic boundary conditions. Black and blue lines mark 1st order transitions. For the correlated metal phase, the Drude weight $\mathcal{D} > 0$, while in all other states $\mathcal{D} = 0$. Dashed red line separates metallic (below) and band insulator (above) states in a model with non-interacting (n-int) d-fermions. At $\Delta = 0$, $\mathcal{D} = \frac{1}{\pi}\sqrt{(2J)^2 - \mu^2}$ for $|\mu| < 2J$ and 0 otherwise. On the left: Drude weight and ground-state energy $\mathcal{E}_0$ for $\Delta = J$ plotted along the arrow in the main panel. Notations are as in Fig. 2. Notice jumps in $\frac{\partial \mathcal{E}_0}{\partial \mu}$ at phase transitions. For $\mu \approx -0.5$ (CDW state), $\mathcal{E}_0$ decreases with increasing n^d_t. For n-int fermions, one has to multiply $\mathcal{D}$ and $\mathcal{E}_0$ (black curves) by 2 due to spin degeneracy, absent for constrained d-fermions.

$\Delta = 0.1J$ and $\Delta = 3J$. Near the s-t resonance, the initial distribution splits into two fast counter-propagating parts with *opposite* transverse local magnetization $\langle T^x_i \rangle$ [Fig. 2(a) and (c)], while for large Δ this splitting is negligible and the state remains practically localized [Fig. 2(b) and (d)]. To understand this behavior, we consider dynamics of a single d-fermion, when the Hamiltonian (4) can be diagonalized in terms of quasiparticles with dispersion $\varepsilon_{k\lambda} = \lambda\rho_k = \lambda\sqrt{(2J\cos k)^2 + \Delta^2}$ ($\lambda = \pm$) [39]. Because these bands have opposite group velocities $v^\lambda_k = \lambda\partial_k\rho_k$, after a time $t > 1/J$ the density has an approximate form $\langle n^d_{i\alpha}(t)\rangle \approx R_\alpha(\xi_-) + L_\alpha(\xi_+)$ where $\xi_\pm = x_i \pm v^-_{k_0}t$, $v^-_{k_0} = -2J|\sin k_0|/\rho_{k_0}$, and L_α, R_α with $\frac{R_s}{L_s} \approx 1$ and $\frac{R_t}{L_t} \approx \left(\frac{\rho_{k_0}-\Delta}{\rho_{k_0}+\Delta}\right)^2$ describe right and left movers. For large Δ, $R_t \ll L_t$ [see Fig. 2(b)]. Similarly, $\langle T^x_i(Jt > 1)\rangle \approx R(\xi_-) + L(\xi_+)$, with $\frac{R}{L} \approx -\frac{\rho_{k_0}-\Delta}{\rho_{k_0}+\Delta} < 0$ [Fig. 2(c)]. This single-particle picture is valid near wavepacket edges with low fermion density [see inset of Fig. 2], and breaks down at the strongly-correlated core.

The correlated metallic state.– To capture interaction effects that lead to correlated metal phase and drive metal-insulator transitions, in Fig. 3 we compute phase diagram of Eq. (4) in 1D, as a function of the detuning Δ and chemical potential μ (described by a term $\delta H_d = -\mu\sum_i n^d_i$). We characterize various GSs with a Drude weight (DW) $\mathcal{D}$ related to the longitudinal conductivity as $\mathrm{Re}\,\sigma_{xx}(\omega \to 0) = \mathcal{D}\delta(\omega)$: $\mathcal{D} > 0$ for a metal and vanishes in an insulator. For a system with periodic boundary conditions, $\mathcal{D} = \frac{1}{N}\frac{d^2\mathcal{E}_0}{d\phi^2}\big|_{\phi=0}$ where $\mathcal{E}_0$ is the GS energy and ϕN is the flux piercing the ring [40, 41]. In Eq. (4) we replace $d^\dagger_{i\alpha}d_{i+1,\beta} \to d^\dagger_{i\alpha}e^{i\phi}d_{i+1,\beta}$ and treat this model using an unbiased DMRG technique [42].

The physics of a non-interacting (n-int) model (4) is determined by filling of single-particle bands $\varepsilon_{k\lambda}$: When μ is inside one of them the system is a metal (regions below dashed red line in Fig. 3), otherwise it is a band insulator [43]. The correlated nature of d-fermions qualitatively changes this picture by dramatically suppressing the metallic phase and transforming the band insulator to either *charge density-wave* (CDW) with $n^d < 1$, or a *triplet Mott state* with $n^d = n^d_t = 1$. Metallic, CDW and Mott phases are separated by a 1st order transition. Surprisingly, a CDW state with $n^d = 0.5$ emerges exactly at $\mu = -\Delta$, right at the metal-insulator transition for non-interacting fermions. While the latter is driven by a simple band filling, the CDW arises due to quantum effects: For $\mu = -\Delta$ the on-site energy of a triplet vanishes which results in a macroscopic degeneracy (associated with different fillings of triplets) of the classical GS. Quantum fluctuations due to s-t virtual hoppings then select a GS with a two-site unit cell. For $n^d > 0.5$ this state evolves into CDWs with larger unit cells.

At low density, one can extract the DW from a group velocity of a wavepacket with small momentum k_0, $v^-_{k_0} \approx \frac{k_0}{m^*}$ [$m^* = \frac{1}{(2J)^2}\sqrt{(2J)^2+\Delta^2}$], as $\mathcal{D}(n^d \ll 1) \approx \frac{n^d}{m^*} = \frac{n^d v^-_{k_0}}{k_0}$.

Discussion.– We studied a FKLM and demonstrated that an interplay between strong on-site FM exchange and AF correlations, each favoring an insulating behavior, allows the small kinetic energy to stabilize a correlated *metallic* phase, whose elementary excitations involve resonating singlet and triplet states of bare local spins and mobile fermions. This s-t mixing leads to a distortion of the AF order and local magnetization *perpendicular* to the Néel vector. We also showed how one can probe this physics in a quantum simulator with AEAs in optical lattices under a laser-induced magnetic field.

Our results, obtained using a low-energy model (4), remain valid within the full Hamiltonian (5) with $\Omega > J$ [44], and should be applicable beyond 1D, because the phases in Fig. 3 are not associated with spontaneous breaking of any continuous symmetry.

The observation of wavepacket dynamics in Fig. 2 and transverse spin excitations does not require temperatures $\sim J$ and relies on an uncorrelated initial triplet state. These features can be probed in quench experiments with AEAs in moving optical lattices [45]. The Drude weight $\mathcal{D}$ can be measured as a response to a weak optical lattice tilt [46]. Thus the phase diagram in Fig. 3 can be verified, at least for low-densities and deep lattices when the band relaxation due to collisions is energetically suppressed.

Acknowledgments.– We thank Ivar Martin for illuminating discussions. This work was supported by NSF (PIF-1211914 and PFC-1125844), AFOSR, AFOSR-

MURI, NIST and ARO individual investigator awards.

[1] P. W. Anderson, Science **177**, 393 (1972).
[2] E. Morosan, D. Natelson, A. H. Nevidomskyy, and Q. Si, Adv. Mater. **24**, 4896 (2012).
[3] E. Dagotto, Science **309**, 257 (2005).
[4] E. Dagotto, New Journal of Physics **7**, 67 (2005).
[5] Y. A. Izyumov and Y. N. Skryabin, Physics-Uspekhi **44**, 109 (2001).
[6] D. M. Edwards, Advances in Physics **51**, 1259 (2002).
[7] P. W. Anderson and H. Hasegawa, Phys. Rev. **100**, 675 (1955).
[8] P. G. de Gennes, Phys. Rev. **118**, 141 (1960).
[9] E. Müller-Hartmann and E. Dagotto, Phys. Rev. B **54**, R6819 (1996).
[10] J. Zang, H. Rder, A. R. Bishop, and S. A. Trugman, Journal of Physics: Condensed Matter **9**, L157 (1997).
[11] R. E. Brunton and D. M. Edwards, Journal of Physics: Condensed Matter **10**, 5421 (1998).
[12] E. Dagotto, S. Yunoki, A. L. Malvezzi, A. Moreo, J. Hu, S. Capponi, D. Poilblanc, and N. Furukawa, Phys. Rev. B **58**, 6414 (1998).
[13] N. Shannon and A. V. Chubukov, Phys. Rev. B **65**, 104418 (2002).
[14] J. Kienert and W. Nolting, Phys. Rev. B **73**, 224405 (2006).
[15] A. V. Gorshkov, M. Hermele, V. Gurarie, C. Xu, P. S. Julienne, J. Ye, P. Zoller, E. Demler, M. D. Lukin, and A. M. Rey, Nat. Phys. **6**, 289 (2010).
[16] X. Zhang, M. Bishof, S. L. Bromley, C. V. Kraus, M. S. Safronova, P. Zoller, A. M. Rey, and J. Ye, Science **345**, 1467 (2014).
[17] G. Cappellini, M. Mancini, G. Pagano, P. Lombardi, L. Livi, M. Siciliani de Cumis, P. Cancio, M. Pizzocaro, D. Calonico, F. Levi, C. Sias, J. Catani, M. Inguscio, and L. Fallani, Phys. Rev. Lett. **113**, 120402 (2014).
[18] F. Scazza, C. Hofrichter, M. Höfer, P. C. De Groot, I. Bloch, and S. Folling, Nat. Phys. **10**, 779 (2014).
[19] G. Pagano, M. Mancini, G. Cappellini, L. Livi, C. Sias, J. Catani, M. Inguscio, and L. Fallani, Phys. Rev. Lett. **115**, 265301 (2015).
[20] M. Höfer, L. Riegger, F. Scazza, C. Hofrichter, D. R. Fernandes, M. M. Parish, J. Levinsen, I. Bloch, and S. Fölling, Phys. Rev. Lett. **115**, 265302 (2015).
[21] R. Zhang, Y. Cheng, H. Zhai, and P. Zhang, Phys. Rev. Lett. **115**, 135301 (2015).
[22] R. Zhang, D. Zhang, Y. Cheng, W. Chen, and H. Z. Peng Zhang, arXiv:1509.01350.
[23] J. Dalibard, F. Gerbier, G. Juzeliūnas, and P. Öhberg, Rev. Mod. Phys. **83**, 1523 (2011).
[24] A. Celi, P. Massignan, J. Ruseckas, N. Goldman, I. B. Spielman, G. Juzeliūnas, and M. Lewenstein, Phys. Rev. Lett. **112**, 043001 (2014).
[25] M. Mancini, G. Pagano, G. Cappellini, L. Livi, M. Rider, J. Catani, C. Sias, P. Zoller, M. Inguscio, M. Dalmonte, and L. Fallani, Science **349**, 1510 (2015).
[26] N. R. Cooper and A. M. Rey, Phys. Rev. A **92**, 021401 (2015).
[27] M. L. Wall, A. P. Koller, S. Li, X. Zhang, N. R. Cooper, J. Ye, and A. M. Rey, Phys. Rev. Lett. **116**, 035301 (2016).
[28] C. D. Batista and G. Ortiz, Advances in Physics **53**, 1 (2004).
[29] See the Supplementary Material, which includes Refs. [24, 25, 35–38, 47–53], for technical details of this calculation.
[30] P. W. Anderson, Journal of Physics C: Solid State Physics **3**, 2436 (1970).
[31] A. Georges, L. de' Medici, and J. Mravlje, Annual Review of Condensed Matter Physics **4**, 137 (2013).
[32] In a 2D optical lattice, the hopping in an excited band generally depends on direction due to different motional states. This complication may be avoided, if uses the third excited band for mobile atoms.
[33] See the Supplementary Material for further details of the cold-atom implementation (5).
[34] See the Supplementary Material for a detailed explanation when one can ignore the doubly-occupied states, and for a calculation of second-order corrections $\sim J_0^2/\Omega$.
[35] U. Schollwöck, Ann. Phys. **326**, 96 (2011).
[36] G. Vidal, Physical Review Letters **93**, 040502 (2004).
[37] S. R. White and A. E. Feiguin, Physical Review Letters **93**, 076401 (2004).
[38] A. J. Daley, C. Kollath, U. Schollwöck, and G. Vidal, Journal of Statistical Mechanics: Theory and Experiment **2004**, P04005 (2004).
[39] See the Supplementary Material for dynamics of single-particle wavepackets.
[40] W. Kohn, Phys. Rev. **133**, A171 (1964).
[41] D. J. Scalapino, S. R. White, and S. Zhang, Phys. Rev. B **47**, 7995 (1993).
[42] See the Supplementary Material for details of DMRG simulations.
[43] See the Supplementary Material for derivation of the Drude weight $\mathcal{D}$ for non-interacting d-fermions.
[44] See the Supplementary Material for a comparison of the wavepacket dynamics in these two cases.
[45] J. Mun, P. Medley, G. K. Campbell, L. G. Marcassa, D. E. Pritchard, and W. Ketterle, Phys. Rev. Lett. **99**, 150604 (2007).
[46] M. Raizen, C. Salomon, and Q. Niu, Physics Today **50**, 30 (1997).
[47] M. Cazalilla and A. Rey, Reports on Progress in Physics **77**, 124401 (2014).
[48] B. K. Stuhl, H.-I. Lu, L. M. Aycock, D. Genkina, and I. B. Spielman, Science **349**, 1514 (2015).
[49] L. Fallani, C. Fort, J. Lye, and M. Inguscio, Opt. Express **13**, 4303 (2005).
[50] H. Katori, M. Takamoto, V. G. Pal'chikov, and V. D. Ovsiannikov, Phys. Rev. Lett. **91**, 173005 (2003).
[51] G. K. Campbell, A. D. Ludlow, S. Blatt, J. W. Thomsen, M. J. Martin, M. H. G. de Miranda, T. Zelevinsky, M. M. Boyd, J. Ye, S. A. Diddams, T. P. Heavner, T. E. Parker, and S. R. Jefferts, Metrologia **45**, 539 (2008).
[52] M. S. Safronova, Z. Zuhrianda, U. I. Safronova, and C. W. Clark, arXiv:1507.06570.
[53] I. Gradshteyn and I. Ryzhik, *Table of Integrals, Series, and Products* (Elsevier Science, 2014).